REPORT DOCUMENTATION PAGE

Form Approved
OMB No. 0704-01-0188

PLEASE DO NOT RETURN YOUR FORM TO THE ABOVE ADDRESS.

1. REPORT DATE *(DD-MM-YYYY)*	2. REPORT TYPE	3. DATES COVERED *(From - To)*
15-11-2008	REPRINT	

4. TITLE AND SUBTITLE

On the anticritical temperature for spacecraft charging

5a. CONTRACT NUMBER

5b. GRANT NUMBER

5c. PROGRAM ELEMENT NUMBER
62601F

6. AUTHORS
Shu T. Lai and Maurice Tautz*

5d. PROJECT NUMBER
5021

5e. TASK NUMBER
RS

5f. WORK UNIT NUMBER
A1

7. PERFORMING ORGANIZATION NAME(S) AND ADDRESS(ES)

Air Force Research Laboratory RVBXT
29 Randolph Road
Hanscom AFB, MA 01731-3010

8. PERFORMING ORGANIZATION REPORT NUMBER
AFRL-RV-HA-TR-2008-1142

9. SPONSORING/MONITORING AGENCY NAME(S) AND ADDRESS(ES)

10. SPONSOR/MONITOR'S ACRONYM(S)
AFRL/RVBXT

11. SPONSOR/MONITOR'S REPORT NUMBER(S)

12. DISTRIBUTION/AVAILABILITY STATEMENT
Approved for Public Release; distribution unlimited.

13. SUPPLEMENTARY NOTES
Reprinted from Journal of Geophysical Research, Vol. 113, A11211, doi:10.1029/2008JA013161, 2008 © 2008 American Geophysical Union.
*AER/Radex, Inc., Lexington, MA

14. ABSTRACT
In recent years, evidence has been found for the existence of a critical temperature for the onset if spacecraft charging to high voltages. High-voltage charging affects scientific instruments on board and is related to spacecraft anomalies. However, less attention has been given to low-voltage charging, which can also affect scientific experiments on board and is relevant to surface chemistry. There also can exist an anticritical temperature for low-voltage spacecraft surface charging. Ambient electrons at very low trempératures tend to cause negative surface charging, albeit at low voltages, and as the electron temperature increases, the charging ceases at a critical value depending on the surface material. We present the theory and numerical results of anticritical temperatures for typical surface materials in Maxwellian space plasmas. The change in anticritical temperature due to a low-incident-energy enhancement of the electron backscatter yield, consistent with recent measurements, is discussed. Approximate expressions for the anticritical temperature upper limits are given on the basis of Taylor expansions at low temperature of the charging onset equation. It is shown that the existence of the anticritical temperature slightly modifies the possible triple-root configurations in the flux-voltage characteristic curve for a material. The surface charging effect of a Maxwellian plasma with flux components spanning the anticritical and critical temperatures is considered. A comparison with an empirical low-voltage charging curve is given.

15. SUBJECT TERMS
Spacecraft charging; Critical temperature; Anticritical temperature; Space plasmas; Secondary electrons; Geosynchronous satellite

16. SECURITY CLASSIFICATION OF:			17. LIMITATION OF ABSTRACT	18. NUMBER OF PAGES	19a. NAME OF RESPONSIBLE PERSON
a. REPORT	b. ABSTRACT	c. THIS PAGE			Shu T. Lai In recent years, evidence has been
UNCL	UNCL	UNCL	Unl	15	19B. TELEPHONE NUMBER *(Include area code)*

Standard Form 298 (Rev. 8/98)
Prescnbed by ANSI Std. Z39.18

JOURNAL OF GEOPHYSICAL RESEARCH, VOL. 113, A11211, doi:10.1029/2008JA013161, 2008

On the anticritical temperature for spacecraft charging

Shu T. Lai[1] and Maurice Tautz[2,3]

Received 11 March 2008; revised 5 June 2008; accepted 18 August 2008; published 15 November 2008.

[1] In recent years, evidence has been found for the existence of a critical temperature for the onset of spacecraft charging to high voltages. High-voltage charging affects scientific instruments on board and is related to spacecraft anomalies. However, less attention has been given to low-voltage charging which can also affect scientific experiments on board and is relevant to surface chemistry. There also can exist an anticritical temperature for low-voltage spacecraft surface charging. Ambient electrons at very low temperatures tend to cause negative surface charging, albeit at low voltages, and as the electron temperature increases, the charging ceases at a critical value depending on the surface material. We present the theory and numerical results of anticritical temperatures for typical surface materials in Maxwellian space plasmas. The change in anticritical temperature due to a low-incident-energy enhancement of the electron backscatter yield, consistent with recent measurements, is discussed. Approximate expressions for the anticritical temperature upper limits are given on the basis of Taylor expansions at low temperature of the charging onset equation. It is shown that that the existence of the anticritical temperature slightly modifies the possible triple-root configurations in the flux-voltage characteristic curve for a material. The surface charging effect of a Maxwellian plasma with flux components spanning the anticritical and critical temperatures is considered. A comparison with an empirical low-voltage charging curve is given.

Citation: Lai, S. T., and M. Tautz (2008), On the anticritical temperature for spacecraft charging, *J. Geophys. Res.*, *113*, A11211, doi:10.1029/2008JA013161.

1. Introduction

[2] In recent years, evidence has been found in support of a critical temperature T^* of ambient electrons for the onset of spacecraft charging at geosynchronous altitudes. The critical temperature is the threshold level for negative voltage charging, based solely on electron currents, assuming a Maxwellian distribution of incident electrons, with accompanying secondary and backscatter interactions in the satellite surface material. The net current, integrated over energy, depends on the temperature of the Maxwellian distribution. The threshold temperature occurs when there is a balance between the primary electron currents entering the material and the secondary/backscatter electrons escaping from it. The solution to this condition yields T^* the critical temperature for the onset of spacecraft charging [*Lai et al.*, 1982, 1983; *Laframboise et al.*, 1982; *Laframboise and Kamitsuma*, 1983; *Lai*, 1991a, 1991b; *Lai and Della-Rose*, 2001; *Lai and Tautz*, 2006].

[3] For many materials, because of the shape of the secondary and backscatter emission curves, there is a second solution at a lower-temperature T_A. The solution, T_A, has the property that surface charging to negative voltages occurs below T_A but is suppressed above it. Because this effect is the opposite to that of the critical temperature, we call T_A the anticritical temperature. In sections 2 and 3, we outline the theory of the critical and anticritical temperatures. Approximate calculations of the anticritical temperature upper limits are presented in section 4. In section 5 we outline the physics of triple root formation and in sections 6 and 7 we study the problem of triple-root jumps and equilibrium spacecraft potentials in a double and triple Maxwellian plasma, assuming that both T_A and T^* exist for a given surface material. Section 8 gives a discussion of the charging effect of a triple-Maxwellian space plasma, having temperature components spanning the anticritical and critical temperatures, with emphasis on the low-voltage spacecraft charging region. In section 9 we give a conclusion.

2. Existence of the Critical Temperature

[4] We first outline the concept of critical temperature. The ambient electron current often exceeds that of ambient ions by nearly 2 orders of magnitude [*Reagan et al.*, 1983] because of the mass difference and thus the ion contribution can be neglected. The onset of spacecraft charging at equilibrium is determined by the balance of incoming and outgoing electron fluxes

$$\int d^3v\, v_n F(\mathrm{v}) = \int d^3v\, v_n [\delta(E) + \eta(E)] F(v), \qquad (1a)$$

[1]Space Vehicles Directorate, Air Force Research Laboratory, Hanscom Air Force Base, Hanscom, Massachusetts, USA.
[2]AER/Radex Inc., Lexington, Massachusetts, USA.
[3]Retired.

0148-0227/08/2008JA013161$09.00

where $F(v)$ is the ambient electron velocity distribution, v_n is the normal component of the electron velocity, and both sides are actually definite integrals. One can write $v_n = v\cos\theta$ in spherical coordinates (v, θ, ϕ), where θ is from 0 to $\pi/2$ and ϕ from 0 to 2π. Writing the integrals explicitly, equation (1a) is of the form

$$\int_0^\infty dv\, v^2 \int_0^{\pi/2} d\theta \sin\theta \int_0^{2\pi} d\varphi v_n F(v) = \int_0^\infty dv\, v^2 \int_0^{\pi/2} d\theta \sin\theta \int_0^{2\pi} d\varphi v_n [\delta(E) + \eta(E)] F(v). \quad (1b)$$

In equation (1a), the secondary and backscattered electron yields, $\delta(E)$ and $\eta(E)$ respectively, are measured in the laboratory as functions of electron energy, E, where $E = (1/2)mv^2$.

[5] To solve equation (1a) for a given surface material, one needs to input the functions $\delta(E)$ and $\eta(E)$. It is convenient to use the fitted $\delta(E)$ function obtained by *Sanders and Inouye* [1978]

$$\delta(E) = c[\exp(-E/a) - \exp(-E/b)], \quad (2)$$

where $a = 4.3\ E_{max}$, $b = 0.367E_{max}$, and $c = 1.37\ \delta_{max}$.

[6] For the backscattered electron yield $\eta(E)$, *Prokopenko and Laframboise* [1980] gave the fitted function

$$\eta(E) = A - B\exp(-CE), \quad (3)$$

where the parameters E_{max}, δ_{max}, A, B, and C depend on the surface material.

[7] Converting to spherical coordinates (E, θ, φ), one can integrate equation (1a) over the energy and the two angular variables. For normal incidence, the angles on both sides of the equation cancel out. After some algebra, one obtains the following equation:

$$\int_0^\infty dEEf(E) = \int_0^\infty dEE[\delta(E) + \eta(E)]f(E), \quad (4)$$

where $f(E)$, obtained from $F(v)$ is the electron distribution with the velocity expressed in terms of energy. For Maxwellian distribution, $f(E)$ is given by

$$f(E) = (n/2mkT)^{3/2}\exp(-E/kT), \quad (5)$$

where n is the electron density, m the electron mass, T the electron temperature, and k the Boltzmann constant. (Strictly speaking, equation (5) is not an energy distribution. There is an energy distribution, which is differently defined [see, e.g., *Mayer and Mayer*, 1963], but we will not need to use it here.) Since the plasma density n is multiplicative, it cancels on both sides of equation (4). Therefore, the threshold condition is independent of the electron density n and depends on the temperature T only. The condition (4) can be written in the equivalent form

$$\frac{\int_0^\infty dEE[\delta(E) + \eta(E)]f(E)}{\int_0^\infty dEEf(E)} = 1. \quad (6a)$$

In shorthand notations, equation (6a) can be written as

$$\langle \delta + \eta \rangle = 1, \quad (6b)$$

where the notations, $\langle$ and $\rangle$, denote averaging in the sense of equation (6a).

[8] Substituting equations (2) and (3) into equation (4), with the distribution function $f(E)$ given by equation (5) and integrating over E, one obtains a sixth-order algebraic equation for kT, corresponding to equation (4)

$$c\left[(1 + kT/a)^{-2} - (1 + kT/b)^{-2}\right] + A - B(C\ kT + 1)^{-2} = 1. \quad (7)$$

A solution of equation (7) can be used to specify the critical temperature T^* [*Lai et al.*, 1982] for the onset of spacecraft charging.

[9] For electrons coming in at various angles, one needs to use angle-dependent δ and η functions. Angle-dependent δ and η functions have been given by *Darlington and Coslett* [1972] and *Prokopenko and Laframboise* [1980], respectively. The algebra becomes more complicated but the physics remains unchanged. Further details on the critical temperature are given by, for example, *Lai and Della-Rose* [2001] and *Lai and Tautz* [2006] and will not be repeated here. For comparison purposes, we include Table 1 listing the critical temperature T^* calculated for several typical surface materials, based on material properties given by *Laframboise and Kamitsuma* [1983]. One can see that kT^* is typically in the few keV range.

[10] There are recent advances in secondary electron yield formulae derived by using laboratory measurements [e.g., *Katz et al.*, 1986; *Cazaux*, 2001, 2006; *Lin and Joy*, 2005; J. R. Dennison, Physics Department, Utah State University, manuscript in preparation]. We are doing a comparative study to assess the effects of the various formulae on the critical temperature. Whenever an improved formula of $\delta(E)$ or $\eta(E)$ becomes available, one can substitute it in equation (4) for updating the numerical value of the critical temperature and the anticritical temperature.

3. Existence of the Anticritical Temperature

[11] Figure 1 shows the yields for the sample material gold as a function of incident energy in the energy range $0 < E < 5$ (keV). The lower curve gives the backscatter yield,

Table 1. Critical Temperature T^*[a]

Material	Isotropic	Normal
Mg	0.4	–
Al	0.6	–
Kapton	0.8	0.5
Al Oxide	2.0	1.2
Teflon	2.1	1.4
Cu-Be	2.1	1.4
Glass	2.2	1.4
SiO_2	2.6	1.7
Silver	2.7	1.2
Mg Oxide	3.6	2.5
Indium Oxide	3.6	2.5
Gold	4.9	2.9
Cu-Be (Activated)	5.3	3.7
MgF_2	10.9	7.8

[a]Units in keV for kT^*.

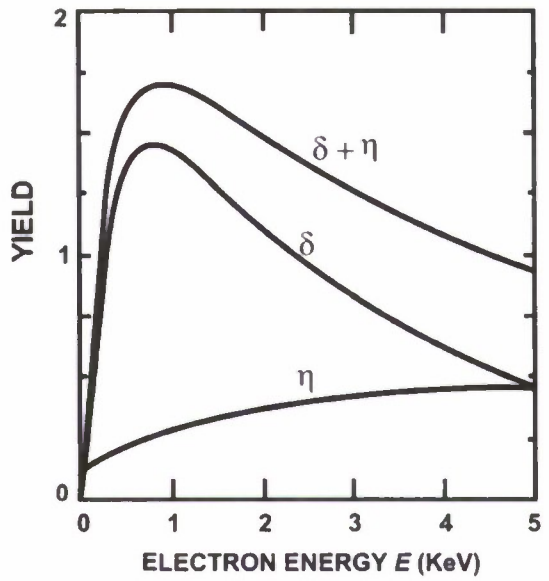

Figure 1. Yield versus energy for gold.

the middle curve the secondary emission and the top curve the summed yield, $\delta(E) + \eta(E)$. It can be seen that at high energies, the total yield goes below unity, giving a negative current contribution, and the integration over energies can produce current balance (see equation (4)) at the critical value T^*. It is apparent from Figure 1 that the "average" yield $\langle \delta + \eta \rangle$ integrated over energy (equation (3)) can also go below unity at low energies and that there could be a second solution. We shall call the unity crossing point ($\langle \delta + \eta \rangle = 1$) at low temperature T_A, the anticritical temperature. The existence and value of T_A depend critically on the low-energy behavior of the yield curves.

[12] Table 2 lists the numerically calculated values of anticritical temperature T_A for some typical surface materials, based on the parameter coefficients of *Sanders and Inouye* [1978] and *Prokopenko and Laframboise* [1980]. It is observed that the kT_A values are mostly below 20 eV for normal incidence and below 10 eV or nearly zero for isotropic incidence. Such low values of anticritical temperature are easily overlooked. From Table 2, we see that the $\delta(E)$ coefficient of some materials, such as gold and silver, has two properties: (1) high values of E_{max} and (2) near unity value of δ_{max}. These two properties give higher values of T_A. The maximum value found is 288 eV for silver at normal incidence.

[13] Since the secondary and backscattered electron emission coefficients $\delta(E)$ and $\eta(E)$ are obtained by fitting data obtained in the laboratory, the signal-to-noise ratio often decreases as the energy E approaches zero, rendering inaccuracies to the fitted data in the low-energy range. Therefore, the coefficients $\delta(E)$ and $\eta(E)$ should not be regarded as highly accurate for small E. In Table 2, anticritical temperatures kT_A below 1 eV are flagged and no value is given. It is also possible that the secondary and backscatter emissions are so small that $\langle \delta(E) + \eta(E) \rangle$ is less than one at all energies. In that case, there would not be a solution for either the critical or anticritical temperature (see materials Mg and Al in the Tables 1 and 2, respectively) and the material should always charge.

[14] The existence of the anticritical temperature T_A stems from the properties of the secondary electron emission coefficient $\delta(E)$ and backscatter coefficient $\eta(E)$. The incident electrons must have enough energy to generate a secondary electron. At sufficiently low-energy E of the incoming electrons, not many exited electrons are created in the material. The result is that the number of incoming (primary) electrons exceeds that of the outgoing secondary electrons and the secondary emission yield goes to zero as E approaches zero. This is not necessarily true for the backscattered electrons. In Figure 1, the backscatter yield goes to a small positive value, which is set by a fit to extrapolated measured data [*Prokopenko and Laframboise*, 1980]. In terms of the backscatter parameters, the yield at $E = 0$ is $A - B$, which for gold is 0.124. However, there are experimental indications that low-energy backscattered particles have a reflection coefficient of one [*Cimino et al.*, 2004] as E goes to zero. This result can also be derived using a quantum mechanics model considering a plane wave electron inci-

Table 2. Anticritical Temperature T_A for Typical Surface Materials[a]

Material	E_{max}	δ_{max}	A	B	C	Isotropic[b]	Normal[b]
Mg	0.25	0.92	0.1460	0.0250	0.3440	—	—
Al	0.30	0.97	0.1568	0.0303	0.3431	—	—
Kapton	0.15	2.10	0.0700	0.0000	0.0000	ε	0.014
Al_2O_3	0.30	2.60	0.1238	0.0172	0.3455	ε	0.020
Teflon	0.30	3.00	0.0900	0.0000	0.0000	ε	0.017
Cu-Be	0.30	2.20	0.3136	0.0692	0.6207	ε	0.020
Glass	0.35	2.35	0.2000	0.0420	0.4100	ε	0.015
SiO_2	0.42	2.50	0.1238	0.0172	0.3435	0.024	0.029
Silver	0.80	1.00	0.3900	0.2890	0.6320	0.184	0.288
Magnesium Oxide	0.40	4.00	0.1238	0.0172	0.3435	ε	0.016
Indium Oxide	0.80	1.80	0.2750	0.0250	0.5400	0.077	0.108
SCATHA Boomat	0.59	1.86	0.4380	0.3250	0.6130	0.041	0.059
Gold	0.80	1.45	0.4802	0.3566	0.6103	0.096	0.114
Cu-Be (Activated)	0.40	5.00	0.3136	0.0692	0.6207	ε	0.010
MgF_2	0.85	6.38	0.1238	0.0172	0.3435	ε	0.019

[a]Anticritical temperature T_A given in keV.
[b]Here — means that there is no T_A, and ε indicates that T_A is below 1 eV.

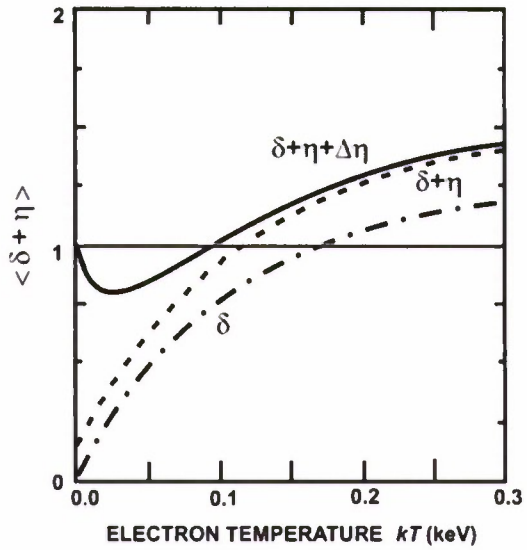

Figure 2a. Current balance equation $\langle \delta + \eta \rangle = 1$ for the antieritieal temperature T_A with and without enhaneed baekseatter for the surface material gold. We have used $E_0 = 0.05$ keV for the enhancement fall-off parameter.

dent on a negative potential step [see, e.g., *Bransden and Joachain*, 1989].

[15] We have ealeulated the yields for gold in the low-energy range $0 < E < 0.3$ (keV), with an added low-energy baekseatter enhancement. The material properties are the same as in Figure 1, except for the additional term

$$\Delta\eta = (1 - A + B)\exp\left(-\frac{E}{E_0}\right), \tag{8}$$

where parameter E_0 specifies the enhaneement fall-off rate. With this change, $\eta(E) + \Delta\eta(E) \rightarrow 1$ as $E \rightarrow 0$ and the same asymptotie baekseatter yield is obtained at large E. Experimental data indieates that E_0 is about 0.05–1.5 keV for gold [*Jablonski et al.*, 1989; *Jablonski and Jiricek*, 1996] and 0.05 keV has been used. The effeet of the added term is to produce a minimum in the summed yield eurve. If this minimum is less than 1.0, an antieritieal temperature T_A exists.

[16] We show in Figure 2a the energy averaged coeffieient $\sigma = \langle \delta + \eta + \Delta\eta \rangle$ for gold as a funetion of kT (keV), with (solid line) and without (dashed line) the additional baekseatter enhaneement term, $\langle \Delta\eta \rangle$

$$\langle \Delta\eta \rangle = (1 - A + B)/(1 + kT/E_0)^2. \tag{9}$$

For referenee, the primary eurve eorresponding to the no baekseatter ease is shown as a dash line. The antieritieal temperature is determined by the intersection of the eurves with the horizontal "negative-to-positive" transition line at $\sigma = 1.0$. With the added term T_A was determined numerieally to be 0.0915, which ean be compared with 0.1143 for the unmodified ease. The T_A value is shifted to lower kT, beeause the σ eurve is elevated by the baekseatter so that the intersection with the horizontal test line oeeurs earlier. The values of antieritieal temperature given in Table 2 thus represent upper limits.

[17] Near the eritieal temperature, there would also be a shift, in this ease to higher kT, though it would be small sinee $\Delta\eta(E)$ falls off rapidly with E. For the ease of gold, we obtain 2.913 for the shifted eritieal temperature and 2.911 for the unmodified ease.

[18] For some materials, the baekseatter enhaneement could be strong enough so that there is no zero erossing in the net averaged flux, $\langle 1 - \delta - \eta \rangle$, eurve and no antieritieal temperature would oeeur. We do not ealeulate a table of modified antieritieal temperatures beeause the parameter E_0 is not generally known experimentally. As indieated in Figure 2b, when E_0 goes to zero, we reeover the unmodified antieritieal temperature. As E_0 inereases, the antieritieal temperature deereases until at some point (here $E_0 \sim 0.13$) it disappears. This type of behavior would oeeur with other materials and the magnitude of the temperature shift ε would depend on the speeifie material parameters. The shift ean be estimated from the eurrent balanee equation, if we expand about kT of the no enhaneement ease. For example, we get for gold

$$\Delta T_A = -\Delta\eta/(d\sigma/dkT) \approx -0.081/3.4 = -0.024. \tag{10}$$

whieh agrees approximately with the antieritieal temperature difference (−0.023) found numerieally. At high kT, in the eritieal temperature region, the derivative $d\sigma/dkT$ changes sign and the enhaneement term is small, leading to a slight positive shift.

[19] There are other baekseattering formulae and measurements published in the literature. They ean slightly affeet the numerieal results. Reeently, *Cimino et al.* [2004] measured the baekseattering of gold and found deviation at near zero energy. In view of this uneertainty, we have done a study using the baekseattering coeffieient for gold as a parameter going over the expeeted range from 0.124 to 1 at near zero energy. Sinee no measurement of other materials is available at near zero energy at this time, we did not pursue this aspeet. The baekseattering equation does not ehange the eoneept of our paper. At this time, Cimino's

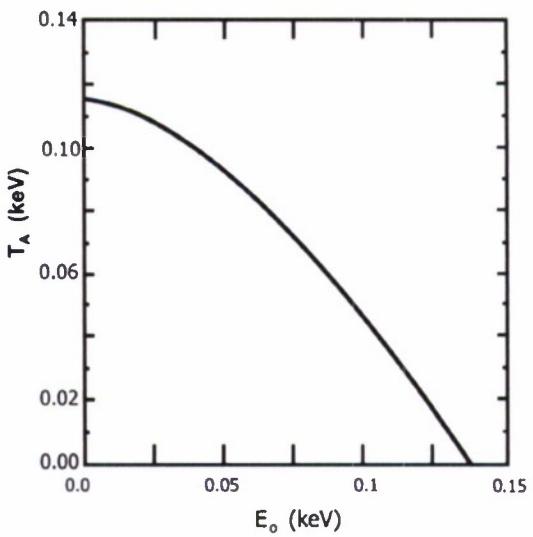

Figure 2b. Antieritieal temperature T_A versus the baekseatter parameter E_0, with gold as the surfaee material.

Table 3. Anticritical Temperature and Three Successive Approximations[a]

Material	kT_A	$kT_0 \pm \%$	$kT_1 \pm \%$	$kT_2 \pm \%$	$kT_3 \pm \%$
Cu-Be (activated)	0.0099	0.0117 +18.7	0.0101 +2.35	0.0099 +0.04	0.0099 +0.09
Kapton	0.0141	0.0105 −25.6	0.0150 +01	0.0140 −0.20	0.0141 +0.64
Mg Oxide	0.0154	0.0146 −4.8	0.0159 +3.50	0.0154 +0.04	0.0154 +0.16
Teflon	0.0168	0.0146 −12.7	0.0176 +4.82	0.0168 +0.01	0.0168 +0.27
MgF_2	0.0192	0.0195 +1.6	0.0196 +2.16	0.0192 +0.05	0.0192 +0.08
Al_2O_3	0.0197	0.0169 −14.3	0.0208 +5.48	0.0197 −0.02	0.0198 +0.35
Cu-Be	0.0197	0.0200 +1.6	0.0207 +5.53	0.0196 −0.02	0.0197 +0.34
Glass	0.0243	0.0218 −10.2	0.0257 +5.74	0.0243 −0.03	0.0244 +0.39
SiO_2	0.0291	0.0246 −15.4	0.0307 +5.72	0.0291 −0.03	0.0292 +0.39
SCATHA Boomat	0.0595	0.0465 −21.9	0.0646 +8.58	0.0593 −0.27	0.0598 +0.49
Indium Oxide	0.1082	0.0837 −22.6	0.1177 +8.85	0.1074 −0.73	0.1094 +1.12
Gold	0.1143	0.0808 −29.3	0.1281 +12.10	0.1132 −0.96	0.1146 +0.31
Silver	0.2873	0.1172 −59.2	0.3237 +12.66	0.2615 −8.99	0.2910 +1.29

[a]Units of the temperatures (multiplied by k) are expressed in keV. Here % is the percent difference from T_A, T_A is the numerical solution with all terms, $T_0 \pm \%$ is the analytical solution neglecting the ion term, $T_1 \pm \%$ is the solution to first order, $T_2 \pm \%$ is the solution to second order, and $T_3 \pm \%$ is the solution to third order.

measurement is the only one available at near zero energy. One can update the numerical values when measurements for more materials are available.

4. Approximate Formula for Anticritical Temperature

[20] A simple approximate formula of T_A in Table 2 is handy for practical purposes. To seek an approximation, we neglect the electron backscattering contribution compared with that of secondary emission. With this change, the current balance equation, equation (7), becomes

$$c\left[(1 + kT/a)^{-2} - (1 + kT/b)^{-2}\right] = 1. \tag{11}$$

By making a Taylor expansion in kT, and keeping only the lowest terms, we get the approximate solution kT_0

$$kT_A \approx kT_0 = \frac{1}{2c}\frac{ab}{(a-b)} \tag{12a}$$

or in terms of E_{max} and δ_{max}

$$kT_0 = 0.147\frac{E_{max}}{\delta_{max}}. \tag{12b}$$

This simple formula is valid at small kT and with no backscatter component.

[21] The kT_0 results obtained from equation (12b) are given in Table 3 for a list of available surface materials (see Table 2 for the properties). In Table 3, the first column specifies the material. The next column, labeled kT_A, is the numerical result. The next two columns show kT_0 and its percent error. It can be seen that, at low anticritical temperatures ($kT < 0.1$ keV) the estimate is accurate to about 20%. But at higher temperatures ($kT > 0.1$ keV), the estimate is considerably worse (silver is $\sim -60\%$). The main reason for this poor kT_0 behavior can be traced to the kT/b term. Since b itself is typically quite small, the approximation of neglecting the higher-order terms progressively fails as kT increases.

[22] We can obtain a better estimate of kT if we develop a hybrid expansion of equation (7). By this we mean that the terms kT/a and CkT are expanded and the first-order terms retained, but all powers of the kT/b term are kept. This procedure leads to the cubic equation shown below

$$\alpha - 1 + 2kT\left(\frac{\alpha}{b} - \beta\right) + (kT)^2\left(\frac{\alpha}{b^2} - \frac{4\beta}{b}\right) - (kT)^3\frac{2\beta}{b^2} = 0, \tag{13}$$

where we have defined $\alpha = 1 + (A - B - 1)/c$ and $\beta = 1/a - BC/c$. This equation can be solved to successive orders by keeping the two lowest-order terms, the first three terms or all four terms. The solutions are denoted by kT_1, kT_2, and kT_3 and the results, along with the percent errors, are shown in Table 3. It is evident that the linear estimate kT_1 is good to about the 10% level and tends to give high values. The quadratic result kT_2 is accurate to about 1%, but it too has 10% errors in the higher-kT range. In order to get the errors down to approximately the 1% level throughout, one needs to solve the cubic equation for kT_3. However, if one requires just a practical "ballpark" estimate of the anticritical temperature the linear result suffices and it is explicitly

$$kT_1 = \frac{b(1-\alpha)}{2(\alpha - b\beta)} = \frac{kT_0(1 - A + B)}{1 + 2kT_0[BC - (1 - A + B)/b]}. \tag{14}$$

This formula contains kT_0 and the extra terms lead to better accuracy than equation (12b). It differs from the pure kT_0 estimate in that backscatter coefficients A, B, C are used and kT/b has been treated more fully. If E_0 is known one can further estimate the effect of backscatter enhancement by employing the shift equation (10).

5. Triple-Root Situation With Two Maxwellian Components

[23] Consider a plasma electron population which is a superposition of two Maxwellian distributions with temperatures T_1 and T_2. A necessary condition [*Lai*, 1991a] for a triple-root situation to occur is

$$T_1 < T^* < T_2, \tag{15}$$

where T^* is the critical temperature. Before we introduce a new degree of complication, the anticritical temperature T_A, into the inequality equation (15), let us first review the underlying idea.

[24] Consider a double Maxwellian distribution $f(E)$ where we have expressed the velocity in terms of the energy E. The electron distributions are

$$f(E) = f_1(E) + f_2(E), \tag{16}$$

$$f_1(E) = n_1\left(m/2\pi kT_{e,1}\right)^{3/2} \exp\left(-E/kT_{e,1}\right), \tag{17}$$

$$f_2(E) = n_2\left(m/2\pi kT_{e,2}\right)^{3/2} \exp\left(-E/kT_{e,2}\right), \tag{18}$$

where $T_{e,1}$ and $T_{e,2}$ denote the first and the second Maxwellian electron temperatures respectively. Three analogous equations can be written for double Maxwellian ions, with the subscript e replaced by i. The temperature in a Maxwellian distribution is defined as the inverse of the slope of the graph of $\log f(E)$ as a function of E. We assume that $T_{e,1} < T_{e,2}$ and $T_{i,1} < T_{i,2}$. For simplicity, we assume charge neutrality, $n = n_e = n_i$. (In the discussion below, variable densities are indirectly accounted for by the varying fluxes.) We temporarily neglect the ions for low potential magnitude. If both temperatures $T_{e,1}$ and $T_{e,2}$ are below T^*, the net flux, integrated over energy and including secondary and backscatter contributions, would be positive. The surface would charge to a positive potential and there is no competition. Likewise, if both $T_{e,1}$ and $T_{e,2}$ are above T^*, the surface would charge to a negative potential and there is again no competition. Therefore, it is necessary to satisfy the inequality (15) for the two distributions to compete with each other. Such competition can produce a triple root situation.

[25] Let us now write down the full expressions of the fluxes collected by a spacecraft at a negative voltage ϕ. The total flux J_T is given by

$$J_T(\phi) = J_1(\phi) + J_2(\phi), \tag{19}$$

where each term is the sum of the separate contributions from the electrons and ions

$$J_1(\phi) = J_{e,1}(\phi) + J_{i,1}(\phi) \tag{20a}$$

$$J_2(\phi) = J_{e,2}(\phi) + J_{i,2}(\phi). \tag{20b}$$

We have explicitly the terms

$$J_1(\phi) = -j_{e,1}(0)[1 - (\delta + \eta)] \exp\left(-\frac{q_e\phi}{kT_{e,1}}\right) + j_{i,1}(0)\left[1 - \frac{q_i\phi}{kT_{i,1}}\right] \tag{21}$$

$$J_2(\phi) = -j_{e,2}(0)[1 - (\delta + \eta)] \exp\left(-\frac{q_e\phi}{kT_{e,2}}\right) + j_{i,2}(0)\left[1 - \frac{q_i\phi}{kT_{i,2}}\right], \tag{22}$$

where

$$\langle \delta + \eta \rangle = \frac{\int_0^\infty dE E f_n(E)[\delta(E) + \eta(E)]}{\int_0^\infty dE E f_n(E)} \qquad (n = 1, 2), \tag{23}$$

$q_e = -e$, and $q_i = +e$.

[26] In equations (21) and (22), $j_{e,n}(\phi)$ and $j_{i,n}(\phi)$ are the ambient electron and ion fluxes, $\delta(E)$ and $\eta(E)$ are the emission coefficients for secondary electrons [e.g., *Sternglass*, 1954a; *Sanders and Inouye*, 1978] and backscattered electrons [e.g., *Sternglass*, 1954b; *Prokopenko and Laframboise*, 1980], and e the elementary charge. The index n (= 1, 2) labels the Maxwellian. The extension to higher-component plasmas would be done by simply including more terms. The exponentials are due to repulsion of electrons by the negative potential (Boltzmann factors) and the square bracketed ion term represents the attraction of positive ions in the orbit-limited regime of *Mott-Smith and Langmuir* [1926], which is a good approximation at geosynchronous altitudes. No approximation of ion mass or temperature relative to those of electrons has been assumed in these terms. In these expressions it is assumed that $\phi < 0$. In the regime $\phi > 0$, the surface would be electron attracting and ion repelling and the net current would rapidly go to negative values.

[27] The symbols in equations (21) and (22) are related to those in equations (20a) and (20b) as follows:

$$J_{e,n}(\phi) = -j_{e,n}(0)[1 - \langle \delta + \eta \rangle] \exp\left(-\frac{q_e\phi}{kT_e}\right) \qquad n = 1, 2 \tag{24}$$

$$J_{i,n}(\phi) = j_{i,n}(0)\left[1 - \frac{q_i\phi}{kT_i}\right] \qquad n = 1, 2. \tag{25}$$

We ignore the ions for ϕ near 0, because $j_{e,n}(0) \gg j_{i,n}(0)$ (n = 1, 2). The flux inequality is usually valid because of the difference in electron and ion masses. We further assume that $j_{e,1}(0) > j_{e,2}(0)$, in order to illustrate the triple root case. The sign convention in equations (20)–(23) is that the incoming electron flux is negative.

[28] The admissible values for the spacecraft potentials are given by the zeros (roots) of the total flux (i.e., given by the current balance equation at steady state)

$$J_T(\phi) = 0. \tag{26}$$

Let us now examine the nature of the function $J_T(\phi)$ by varying ϕ. At $\phi = 0$, $J_T(\phi = 0)$ is dominated by the contribution from the electron term of the first Maxwellian distribution

$$J_T(0) \approx -j_{e,1}(0)[1 - (\delta + \eta)]. \tag{27}$$

Since $T_1 < T^*$ (equation (15)), there are more outgoing electrons than incoming ones, thereby rendering $\langle \delta + \eta \rangle$ greater than unity and therefore $J_T(0)$ is positive. This situation is depicted in Figure 3 (top).

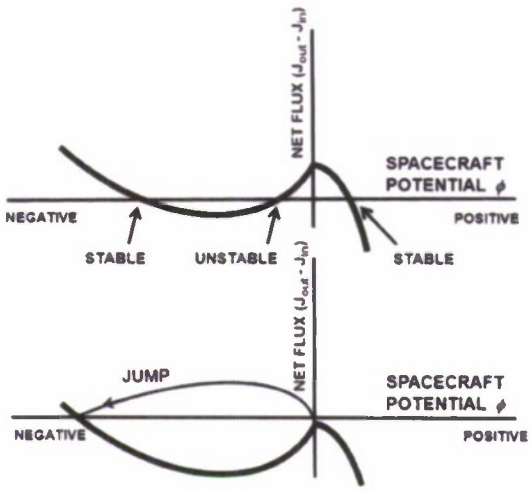

Figure 3. A (top) triple-root situation and (bottom) triple-root jump in spaeeeraft potential ϕ for a double-Maxwellian distribution of eleetrons in spaee. The roots are at the zeros of the total flux. The $J_T(\phi)$ eurve for $\phi > 0$ follows a different equation for eleetron attraetion and ion repulsion.

[29] As the magnitude of ϕ (<0) inereases, the exponentials in equations (21) and (22) beeome inereasingly influential. Sinee $T_1 < T_2$, the exponential in equation (21) deereases faster than that in equation (22) and $J_T(\phi < 0)$ deereases. Eventually, at suffieiently large magnitude of ϕ (<0), $J_T(\phi < 0)$ is dominated by the eontribution from the eleetron term of the seeond Maxwellian distribution. Sinee $T_2 > T^*$, the $\langle \delta + \eta \rangle$ term in equation (27) is less than unity, rendering $J_T(\phi < 0)$ negative (Figure 3 (top)).

$$J_T(\phi < 0) = -j_{e,2}(0)[1 - \langle \delta + \eta \rangle] \exp\left(-\frac{q_e \phi}{kT_{e,2}}\right). \tag{28}$$

As the magnitude of ϕ (<0) inereases further, eventually the ion terms in equations (21) and (22) will beeome inereasingly important. This is beeause more and more positive ions are attraeted by the inereasingly negative potential $\phi(\ll 0)$. This results in the total fluxes $J_T(\phi < 0)$ rising to positive values (Figure 3) and subsequently.

[30] As the environment parameters ehange in time, the flux-voltage eurve adjusts aeeordingly. If the net flux deereases or inereases through zero, a pair of neighboring roots ean sometimes eoalesee and disappear. If this happens, a jump in spaeeeraft potential to the remaining root would oeeur (Figure 3 (bottom)). In a general plasma, there may be more than three roots. The even roots are stable and the odd roots are unstable [*Lai*, 1991a]. If the dynamie plasma ehanges sueh that two roots eoalesee, the jump is between two remaining stable roots.

[31] The prerequisites for a triple root jump are: a positive flux near the origin ($\phi <$ but ≈ 0), with a deerease to negative flux at middle potentials ϕ(<0), followed by the rise to positive flux in the limit ($\phi \ll 0$). If the positive flux at low potentials ϕ(<0) goes negative or the negative flux at the middle potentials goes positive, two of the roots ean disappear and a jump to the remaining stable root triggered.

6. Double-Maxwellian Distribution With a Low-Temperature Component

[32] Now let us look at spaeeeraft eharging when there is a double-Maxwellian plasma with a eomponent that has temperature less than the antieritieal level. For brevity, we label the eleetron terms by their uneharged strength $j_n = |J_{e,n}(0)|$ where $n = 1, 2$ eorresponding to the nth temperature.

6.1. Case 1

[33] Consider a double-Maxwellian distribution in whieh the two temperatures T_0 and T_1 satisfy the following inequality:

$$T_0 < T_A < T_1 < T^*. \tag{29}$$

We initially assume that at $\phi = 0$, the dominant eontribution is from j_0, whose temperature T_0 satisfies equation (29), and therefore $J_T(0)$ is negative. As the magnitude of ϕ(<0) inereases, the exponential term multiplying j_0 deereases faster than that multiplying j_1. Eventually, the seeond distribution ($T = T_1$) gains the upper hand. The seeond distribution has $T_A < T_1 < T^*$ (equation (29)) and therefore $J_T(\phi < 0)$ ean be pushed from negative to positive. As the magnitude of ϕ(<0) inereases further, eventually the ineoming ion flux will win beeause a high negative voltage attraets abundant positive ions. Therefore, $J_T(\phi \ll 0)$ goes more positive. We eonelude that the situation of equation (29) does not feature a triple root. There is only a single negative root, whieh arises when the j_0 term pushes the net flux down to negative values. This situation is illustrated in Figure 4f. If the j_0 term is not strong enough to drive the net flux to negative values, the root would form at positive potential. If the j_1 term is negligible, the flux eurve would match the ion line until the j_0 term eomes in. On the other hand, if at $\phi = 0$, the dominant eontribution is from j_1, then the eurrent is initially positive and stays positive. There is again no triple root situation and a single root would form at positive potentials.

[34] Consider now the ease where the ambient plasma ehanges sueh that the j_1 flux inereases. The net flux is lifted higher and any existing negative root would move toward the origin (less negative).

6.2. Case 2

[35] Consider a double-Maxwellian distribution in whieh the two temperatures T_0 and T_2 satisfy the following inequality:

$$T_0 < T_A < T^* < T_2. \tag{30}$$

We initially assume the first Maxwellian distribution be more abundant. At $\phi = 0$, the dominant eontribution is from j_0, whose temperature T_0 satisfies equation (30) and therefore $J_T(0)$ is negative. As the magnitude of ϕ(<0) inereases, the first exponential (equation (21)) loses its influenee eompared with that of the seeond (equation (22)). Eventually, the seeond Maxwellian gains the upper hand.

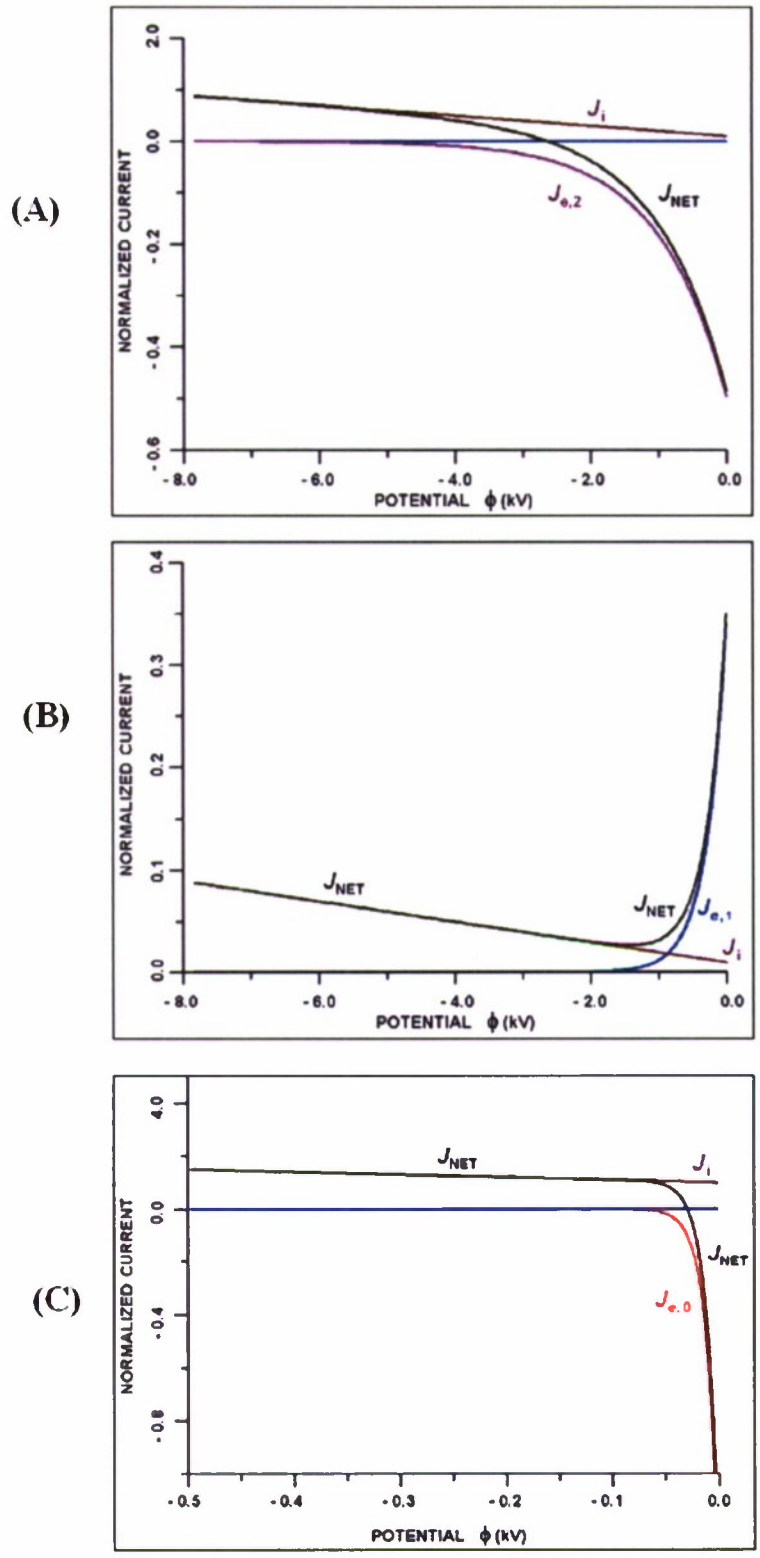

Figure 4. (a) Current-voltage behavior in a single-Maxwellian plasma. The inputs are listed in Table 4 (ease a). (b) Current-voltage behavior in a single-Maxwellian plasma. The inputs are listed in Table 4 (case b). (c) Current-voltage behavior in a single-Maxwellian plasma. The inputs are listed in Table 4 (ease e). (d–g) Current-voltage behavior in double- or triple-Maxwellian plasma. The inputs are listed in Table 4 (eases d–g).

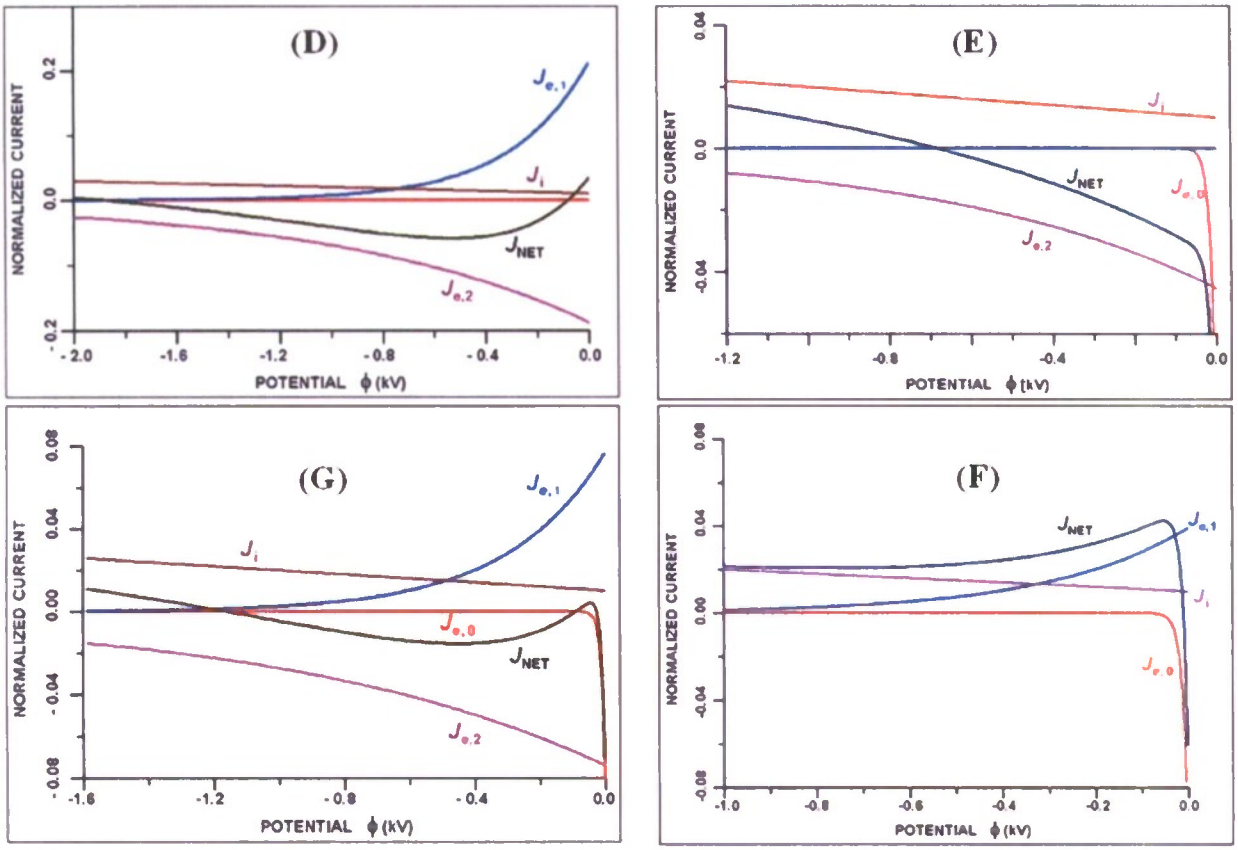

Figure 4. (continued)

However, the second Maxwellian distribution ($T_2 > T^*$) also favors negative flux. Therefore, both Maxwellian distributions behave in the same way: both j_0 and j_2 give negative flux and there is no competition between the distributions. As ϕ (<0) increases further, the incoming ion flux dominates because high negative voltages attract positive ions. We conclude that in this case there is no triple-root situation. There is only a single negative root, arising when the term j_0 plus the term j_2 push the net flux to negative values. The characteristic curve is shown in Figure 4e. If these combined terms are not strong enough to drive the net flux to negative values, the root would form at positive potential.

[36] If j_2 increases, as the plasma evolves, the net flux decreases. A root at negative potential would move toward more negative potentials. If j_2 is strong enough to produce a negative root without a j_0 contribution, the root can move to high negative potentials. This is the normal case for charging above the critical temperature (Figure 4a).

7. Triple-Maxwellian Distribution With a Low-Temperature Component

[37] Consider a triple-Maxwellian distribution in which the three temperatures satisfy the following inequality:

$$T_0 < T_A < T_1 < T^* < T_2. \tag{31}$$

The equation (19) is now generalized to

$$J_T(\phi) = J_0(\phi) + J_1(\phi) + J_2(\phi), \tag{32}$$

where the terms have the forms given in equations (21)–(23). As in section 6, we assume that each of the electron fluxes is about 2 orders of magnitude higher than the corresponding ion fluxes. Let us assume further that the first Maxwellian electron flux $j_{e,0}(0)$ is stronger than the second and third electron fluxes. Accordingly, at $\phi = 0$, the total flux $J_T(0)$ is negative, and a representative point, A, is shown in Figure 5.

[38] As ϕ(<0) increases in magnitude, the low-temperatures $T_{e,0}$ in the denominator of the exponential reduces the low-energy flux $j_{e,0}(\phi)$ faster than the middle energy flux $j_{e,1}(\phi)$. Eventually, $j_{e,1}(\phi)$ exceeds $j_{e,0}(\phi)$ and can dominate. Since the temperature $T_{e,1}$ of $j_{e,1}(\phi)$ is below the critical temperature T^*, the contribution is positive. In other words, the total flux $J_T(\varphi)$ can be driven positive. A representative point B is shown in Figure 5.

[39] As ϕ(<0) increases further in magnitude, the exponential of $J_1(\phi)$ in equation (32) will diminish faster than that of $J_2(\phi)$ in equation (32) because $T_{e,1} < T_{e,2}$. When $J_2(\phi)$ dominates, charging to negative voltages will occur because T_2 exceeds the critical temperature T*. As a result, the total flux, $J_T(\phi)$, can go negative. A representative point C is shown in Figure 5.

[40] As ϕ(<0) increases even further in magnitude, eventually the increasing highly negative potential ϕ will attract

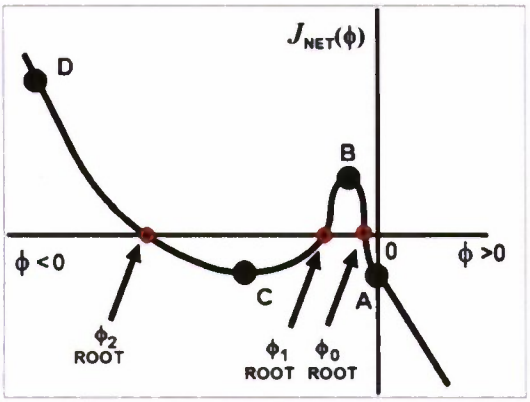

Figure 5. A triple-root situation for a triple-Maxwellian distribution of electrons in space. As the space environment changes, the distributions change. Suppose the spacecraft surface potential is at the first root ϕ_0 on the right (near 0) initially. Let the point near B change in such a way that it sinks as time evolves. When it sinks below $J_T(\phi) = 0$, the first two roots ϕ_0 and ϕ_1 coalesce and disappear together, leaving only the third root ϕ_2 at the far left (high $\phi < 0$). The spacecraft potential would jump to the third root ϕ_2.

so many incoming ions that the ion flux will dominate over the fluxes of electrons. When the incoming ion flux dominates, the total flux $J_T(\phi)$ will be positive. Further increases in the magnitude of ϕ (<0) will not alter the dominance of the ions. A representative point D is shown in Figure 5.

[41] The curve in Figure 5 illustrates a possible initial flux-voltage characteristic compatible with the plasma temperature condition (equation (31)). As the plasma evolves in time, the flux j_1 could decrease or j_2 could increase, causing the positive bump in the flux-voltage curve (at point B) to drop down to negative current. If the surface was originally lying at the root between B and A, it would jump to the high negative root between points C and D.

[42] In Figure 6 we show a case where the j_1/j_2 ratio is low enough to lower the net flux near the origin to slightly negative values. It is evident that no triple root is possible, but that one could occur if there was no j_0 component pulling down the curve at the origin (so the plot looks like Figure 3 (top)). It is in special cases like this one that the T_0 term makes a difference in the possible appearance of triple roots.

[43] This discussion illustrates that, depending on the relative magnitudes of the fluxes, a triple root situation can develop when the plasma temperatures span the critical and anticritical temperatures. The anticritical component produces a negative down turn in the flux-voltage characteristic curve, near the origin. It only slightly modifies the triple root situation relative to the double Maxwellian case and the formation of triple roots still depends primarily on the relative strengths of the j_1 and j_2 fluxes. A more quantitative numerical treatment of the threshold for the triple root situations is described in Appendix A.

8. Anticritical Temperature and Low-Voltage Charging

[44] In this section we describe the possible shape of a low-voltage surface charging curve plotted against the average electron temperature. We will assume that the spacecraft is differentially charged and that there is a cloud of low-energy electrons present. The electron cloud could form because of secondary electrons trapped locally or because of returning photoelectrons in sunlight. The mechanisms of low-energy electron cloud formation are outside the scope of this paper.

[45] We consider a plasma distribution with three possible Maxwellian components, with relative flux strengths J_0, J_1, J_2. The charging is discussed with respect to the average electron temperature. Let the overall plasma temperature T be given by the flux-weighted expression.

$$T = \frac{j_0 T_0 + j_1 T_1 + j_2 T_2}{j_0 + j_1 + j_2}. \tag{33}$$

Let us look first, at the lowest average temperature region. The flux is dominated by electrons with temperature in the anticritical region. The potential is set mainly by a balance between the low-temperature electrons with strength J_0 and the ions. This situation is described in Figure 4c, with negligible J_1 contribution. The electrons add a negative contribution near the origin and if the strength J_0 is sufficient to turn the net flux into negative values, there will be a root formed. If the electron flux is not strong enough, the flux will be positive at the origin, and the root will form at positive voltage. Let us now consider the case where the average electron temperature is above the anticritical temperature, but below the critical temperature. We can represent this situation by adding a substantial positive contribution of strength J_1 from a Maxwellian term with temperature above anticritical. The effect of this term is to bump the J_{NET} curve up until it reaches the point at which the low-energy electrons come in and again produce a drop to negative flux near the origin (see Figure 4f). We note that a rising bump due to J_1 would cause the root to move slightly toward the origin. Consider now the case with the average electron temperature well above the critical temperature. A dominant electron flux of strength J_2 would pull the net flux curve to negative values. If there is any small low-energy J_0 contribution still present, it would have a little effect on the root. The transition from the situation of Figure 4f to the present case (of rising electron temperature resulting in J_2 dominating), is shown in Figure 6. For the purpose of illustrating the transition from Figure 6 (top) to Figure 6 (bottom), we have highlighted the J_{NET} curve. There would be an approximately linear rise in the charging potential above the critical temperature as can be predicted from a simple single Maxwellian model [*Lai and Tautz*, 2006].

[46] The case where the average electron temperature is approximately equal to the critical temperature can be quite complex. In this region one expects to get both J_1 and J_2 contributions and the result is sensitive to the ratio J_1/J_2. If J_1 is stronger than J_2, a triple root situation can occur, as depicted in Figure 5. If J_1 is weaker than J_2 one can obtain the curve shown in Figure 6 (bottom), where the J_1 term is not strong enough to push the net flux to positive values and a single root forms. In this complex case, the threshold for the triple root formation depends on the temperatures as well as the ratio J_1/J_2 and is not very sensitive to j_0. In the limit $T_1 \rightarrow T_2 = T^*$, the high-temperature electron fluxes

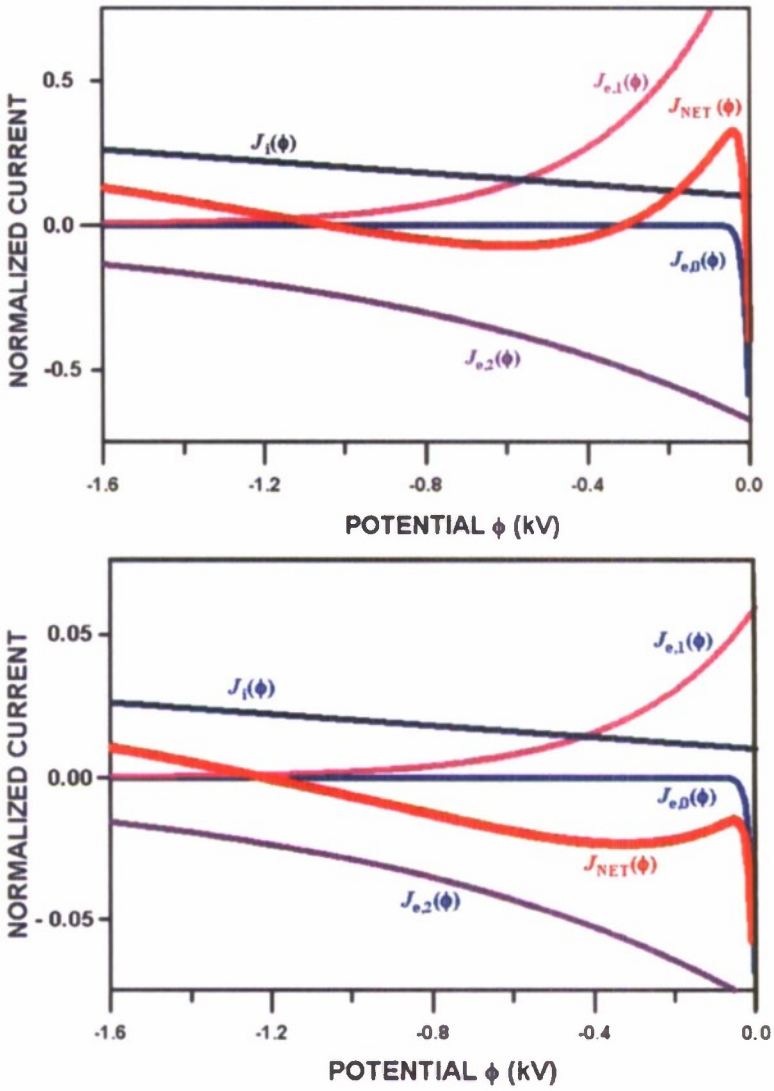

Figure 6. Transition from (top) a triple-root situation to (bottom) a single-root situation. The inputs are $kT_0 = 0.11$, $kT_2 = 0.3$, and $kT_3 = 0.1$ keV. The density inputs are $n_0 = 4$, $n_1 = 0.4$ (in Figure 6 (top)), $n_1 = 0.2$ (in Figure 6 (bottom)), and $n_2 = 0.1$ cm^{-3}. The ion temperature $kT_i = 1$ keV and the ratio of ion current to electron current is taken as 0.01.

tend to cancel and one reverts to the previous low-energy case (Figure 4a).

[47] For comparison, we have grouped together the complete set of seven different cases of current-voltage behaviors in Figures 4a–4g. The equations used are equations (28) and (29) or their respective simplifications for double and single Maxwellian cases. The density and temperature inputs are listed in Table 4.

[48] We remark that near T^*, the current-voltage curve tends to be nearly flat. A slight "pulling up" and a "push down" near the zero crossing may make a triple root situation to appear. For a triple root, we need a positive flux J_1 at $T_1 < T^*$ in comparison with a negative flux J_2 at $T_2 > T_1$. One can write $T_1 = T^* - \Delta_1$ and $T_2 = T^* + \Delta_2$. Since Δ_1 and Δ_2 do not have to be equal or small, it is difficult to make a general statement on the triple root location. Suppose a triple root situation forms as a result. The corresponding signed fluxes J_0 and J_2 are negative because of our temperature assumptions. The flux j_0 can be smaller than j_1 and j_2, because its velocity is much slower than the others. In the average temperature T, the flux $j_0 \sim 0$ in equation (33), so that

$$T = \frac{j_1 T_1 + j_2 T_2}{j_1 + j_2}. \tag{34}$$

If $j_1 \approx j_2$, equation (34) becomes

$$T = \frac{1}{2}(T_1 + T_2), \tag{35}$$

and assuming $\Delta_1 \approx \Delta_2$ or small with respect to T^*, then equation (35) becomes $T \approx T^*$.

[49] In Figure 7 we show empirical data for the negative of the measured spacecraft potential versus average electron

Table 4. Electron Density Input in Case Studies[a]

Case	n_0	n_1	n_2
a	0.0	0.0	0.1
b	0.0	0.1	0.0
c	1.0	0.0	0.0
d	0.0	0.3	0.1
e	4.0	0.0	0.1
f	4.0	0.2	0.0
g	4.0	0.275	0.1

[a]Input densities n_0, n_1, and n_2 (cm^{-3}) for three Maxwellian distributions with temperatures $T_0 < T_A < T_1 < T^* < T_2$, respectively. For the calculations in Figures 4a–4g, we have used $kT_0 = 0.011$ keV, $kT_A = 0.014$ keV, $kT_1 = 0.3$ keV, $kT^* = 0.5$ keV, and $kT_2 = 0.9$ keVs. The kapton values of T_A, T^*, secondary electron coefficient, and backscattered electron coefficient are used.

temperature of the ambient plasma, obtained on a Los Alamos National Laboratory (LANL) satellite under eclipse conditions [*Thomsen et al.*, 1999]. We have provided above a qualitative physical interpretation to the data. Only two electron distributions plus ions are needed to describe the main features of Figure 7. At low average temperatures, low negative charging can occur. As the average temperature rises above the anticritical level (here estimated at $\sim$ 10 eV), positive flux comes in and lifts the net flux curve, shifting negative roots to smaller values. This shift to smaller negative charging voltages is seen statistically in Figure 7. As the average temperature goes above the critical temperature ($\sim$300 eV), the negative flux begins to dominate and a linear response to high (negative) potentials is seen. Triple root configurations can occur when the average temperature is near the critical temperature and the high (negative) potentials seen in Figure 7 at about 300 eV have the signature of triple root jumps.

9. Conclusion

[50] For many surface materials an anticritical temperature exists along with the well-known critical temperature for onset of negative charging. The anticritical temperature allows low-voltage negative charging to occur below it and suppresses the charging above it. These two temperatures occur because of the characteristic shapes of the secondary and backscatter yield curves and the theory for each is similar (current balance). While the critical temperatures for materials charging are of the order of a kilovolt, the anticritical temperatures, if they exist, are typically less than a few hundred volts. There is a large uncertainty in the anticritical temperature due to the unknown behavior of the electron backscatter as the incident energy goes to zero. Reliable values of anticritical temperature await the development of more accurate electron backscatter measurements. In theory, a low-energy enhancement in the backscatter yield moves the anticritical temperature to smaller values and it vanishes if the backscatter is too strong. Due to the low energies involved, approximate values of the anticritical temperature can be obtained by Taylor expansions, but these are also subject to the same backscatter uncertainties. We have looked systematically at low-energy charging with a double and triple Maxwellian plasma. The low-energy charging versus electron temperature is described qualitatively and is in approximate agreement with a sample of LANL measured data. Triple root situations are also discussed and a rough signature is given; anomalous charging occurs just below the critical temperature. Charging points having this approximate triple root signature are also seen in the sample data.

Appendix A: Thresholds for Triple-Root Formation

[51] We consider a triple Maxwellian plasma with temperatures T_0, T_1, and T_2 which satisfy

$$T_0 < T_A < T_1 < T^* < T_2,$$

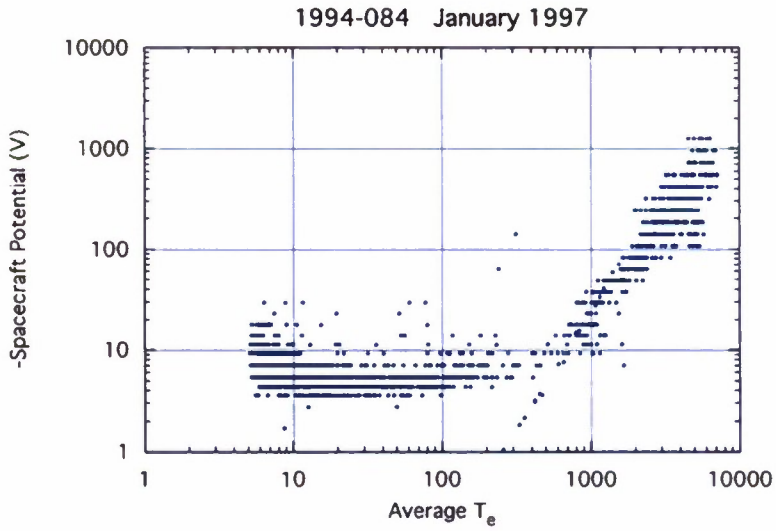

Figure 7. LANL spacecraft charging versus average electron temperature. The data is for eclipse. A rough estimate of the anticritical temperature kT_A is 10 eV, and a rough estimate of the critical temperature kT^* is 300 eV. (Courtesy of M. F. Thomsen.)

where T_A and T^* are the anticritical and critical temperatures for charging. We can write the total incoming flux, in the orbit-limited regime, as

$$J_T(\phi) = J_0 \exp\left(-\frac{q_e\phi}{kT_0}\right) + J_1 \exp\left(-\frac{q_e\phi}{kT_1}\right) + J_2 \exp\left(-\frac{q_e\phi}{kT_2}\right) + J_i\left(1 - \frac{q_i\phi}{kT_i}\right), \quad \text{(A1)}$$

where q_e is the electron charge, q_i the ion charge, and $\phi < 0$ the surface potential. The positive ion flux J_i given in the last term of equation (A1) is typically much smaller than the electron fluxes, at low charging potentials, and we shall neglect it in the (necessary) threshold condition. The J_N (N = 0, 1, 2) are the signed electron fluxes at zero potential. In terms of the variables in the main text, we have

$$J_N = -j_{eN}(0)(1 - \langle\delta + \eta\rangle),$$

where δ and η are the corresponding secondary and backscatter coefficients. According to our temperature assumption, the signs of J_0 and J_2 are negative and that of J_1 is positive. As in the text, we can introduce the absolute flux strengths $j_N = |J_N|$. We can then write equation (A1) as

$$j(\phi) = -j_0 \exp\left(-\frac{q_e\phi}{kT_0}\right) + j_1 \exp\left(-\frac{q_e\phi}{kT_1}\right) - j_2 \exp\left(-\frac{q_e\phi}{kT_2}\right). \quad \text{(A2)}$$

In equation (A2), the electron potential energy $q_e\phi$ is positive for negative charging voltages. The signs of the terms are given explicitly. We could normalize to the central region flux, making $j_1 = 1$, since this term must always be present for triple root formation. If there is no j_0 flux present, a necessary condition for a triple root situation is simply that the flux be positive at the origin ($\phi = 0$) so that the strengths satisfy $j_1 > j_2$ [see *Lai*, 1991a]. If there is a j_0 component, this threshold condition will be modified, as is discussed below.

[52] A necessary condition for a triple root situation to occur is that the net flux-voltage characteristic goes positive near the origin and then sink to negative values at larger $q_e\phi$. If the ions are neglected, this condition can be satisfied if the electron curve has a maximum at some point $q_e\phi_1$ and a minimum at $q_e\phi_2 > q_e\phi_1$. We can write these extrema conditions as

$$\frac{1}{q_e}\left(\frac{dj}{d\phi_1}\right) = \frac{j_0}{kT_0}\exp\left(-\frac{q_e\phi_1}{kT_0}\right) - \frac{j_1}{kT_1}\exp\left(-\frac{q_e\phi_1}{kT_1}\right) + \frac{j_2}{kT_2}\exp\left(-\frac{q_e\phi_1}{kT_2}\right) = 0 \quad \text{(A3)}$$

$$\frac{1}{q_e}\left(\frac{dj}{d\phi_2}\right) = \frac{j_0}{kT_0}\exp\left(-\frac{q_e\phi_2}{kT_0}\right) - \frac{j_1}{kT_1}\exp\left(-\frac{q_e\phi_2}{kT_1}\right) + \frac{j_2}{kT_2}\exp\left(-\frac{q_e\phi_2}{kT_2}\right) = 0. \quad \text{(A4)}$$

For the purposes of numerical analysis, we can regard these conditions as two equations in the unknowns $f_0 = j_0/j_1$ and $f_2 = j_2/j_1$, with T_0, T_1, T_2, $q_e\phi_1$, $q_e\phi_2$ as fixed parameters. A simple matrix inversion then yields the solutions

$$\begin{pmatrix} f_0 \\ f_2 \end{pmatrix} = \frac{1}{kT_1}(M)^{-1}\begin{pmatrix} \exp(-q_e\phi_1/kT_1) \\ \exp(-q_e\phi_2/kT_1) \end{pmatrix}, \quad \text{(A5)}$$

where (M) is the 2 × 2 matrix

$$(M) = \begin{pmatrix} \frac{1}{kT_0}\exp\left(-\frac{q_e\phi_1}{kT_0}\right) & \frac{1}{kT_2}\exp\left(-\frac{q_e\phi_1}{kT_2}\right) \\ \frac{1}{kT_0}\exp\left(-\frac{q_e\phi_2}{kT_0}\right) & \frac{1}{kT_2}\exp\left(-\frac{q_e\phi_2}{kT_2}\right) \end{pmatrix}. \quad \text{(A6)}$$

This procedure yields the variables f_0 and f_2 as functions of the temperatures and potential energies. If j_1 is known, then by substitution in equation (A2) we further obtain $j(\phi_1)$ and $j(\phi_2)$. To illustrate the numerics, we assume nominal temperatures (keV) for the regions: $kT_0 = 0.011$, $kT_1 = 0.3$, and $kT_2 = 1.0$. We have calculated the difference $q_e d\phi = q_e\phi_2 - q_e\phi_1$ with $j(\phi_1)$ held at zero. This gives the $d\phi$ dependence at the (necessary) threshold. The calculation indicates that $d\phi$ is approximately a constant at the threshold. Its value depends on the chosen temperatures.

[53] In order to better understand the onset of triple root formation, we examine the approximate behavior at the threshold condition.

$$\frac{j(\phi_1)}{j_1} = -f_0\exp\left(-\frac{q_e\phi_1}{kT_0}\right) + \exp\left(-\frac{q_e\phi_1}{kT_1}\right) - f_2\exp\left(-\frac{q_e\phi_1}{kT_2}\right) = 0. \quad \text{(A7)}$$

If $q_e\phi_1 \gg kT_0$ we can neglect the first term in (A.7) and find

$$f_2 = \exp\left(-\frac{q_e\phi_1}{kT_{21}}\right), \quad \text{(A8)}$$

where we have defined the temperature variable $T_{21} > 0$ as

$$T_{21} = \frac{T_2T_1}{(T_2 - T_1)}. \quad \text{(A9)}$$

Now let us look for another approximate expression for f_2. From the matrix solution, we have

$$f_2 = \frac{M_{21}^{-1}}{kT_1}\exp\left(-\frac{q_e\phi_1}{kT_1}\right) + \frac{M_{22}^{-1}}{kT_1}\exp\left(-\frac{q_e\phi_2}{kT_1}\right). \quad \text{(A10)}$$

If $q_e\phi_1 \gg \mathrm{kT_0}$, we can again neglect the first term. We are left with

$$f_2 \sim \frac{T_2}{T_1}\exp\left(\frac{q_e\phi_2}{kT_{21}}\right). \quad \text{(A11)}$$

Combining equation (A11) with equation (A8) we get

$$q_e d\phi = q_e\phi_2 - q_e\phi_1 = kT_{21}\log\left(\frac{T_2}{T_1}\right). \quad \text{(A12)}$$

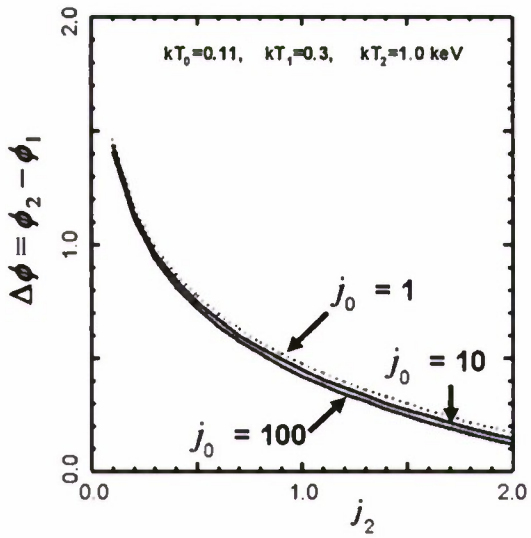

Figure A1. Estimated $\Delta\phi = \phi_2 - \phi_1$ versus j_2, with j_0 as fixed parameter, for nominal temperatures.

This expression corresponds to the numerical result of constant $q_e d\phi$.

[54] In a physical case, we are more likely to know the fluxes j_0, j_1, j_2 than the positions of the extrema ϕ_1 and ϕ_2. Using equations (A3) or (A4), approximate expressions for ϕ_1 and ϕ_2 can be obtained in terms of temperatures and fluxes. An approximation for ϕ_1, is found by putting the exponential in the last term of equation (A3) equal to one, which yields

$$q_e\phi_1 = kT_{01}\log\left(\frac{T_0}{j_0}\left(\frac{j_1}{T_1} - \frac{j_2}{T_2}\right)\right). \tag{A13}$$

where $T_{01} < 0$ is defined in the same way as in equation (A9). We can get an approximate expression for ϕ_2, by neglecting the first term in equation (A4), which gives

$$q_e\phi_2 = kT_{21}\log\left(\frac{j_1 T_2}{j_2 T_1}\right). \tag{A14}$$

In these approximations, the log argument and $q_e\phi_1$, $q_e\phi_2$ are positive, leading to restrictions on the flux strengths ($j_0/T_0 + j_2/T_2 < j_1/T_1, j_2/j_1 < T_2/T_1$). When a representative set of parameters T_0, T_1, T_2 and j_0, j_1, j_2 are known, equations (A13) and (A14) can be used to estimate ϕ_1, ϕ_2 and if the condition

$$q_e\phi_2 - q_e\phi_1 > kT_{21}\log\frac{T_2}{T_1} \tag{A15}$$

holds, then, to the level of approximation considered, the system is above the threshold. If we again let the temperatures have the nominal values given above, the value of the right hand side of equation (A15) is found to be 0.52.

[55] Using the approximate formulae (equations (A13)–(A15)) we can estimate the threshold behavior directly as a function of the flux strengths. In Figure A1, we show the variable $d\phi$ as a function of j_2, over three decades of j_0 (in this plot we assume $j_1 = 1$). There is very little j_0 dependence. At the threshold ($d\phi = 0.52$) it is evident that j_2 is slightly less than one. Lower values of j_2 are above threshold and higher values are below it. Figure A1 indicates a rough signature for triple root charging: there should be a positive flux contribution from below the critical temperature and a weaker negative (here $j_2 < 1$) flux from above the critical temperature. On a plot of spacecraft charging versus the average electron temperature, the triple root potentials would appear as uncharacteristic high (negative) potentials occurring below the critical temperature.

[56] The threshold relation investigated in this appendix is a necessary condition. To obtain both necessary and sufficient conditions one must include the ions. Thus, to get a triple root situation, we would have

$$j(q_e\phi_1) + J_i(q_i\phi_1) > 0 \tag{A16a}$$

$$j(q_e\phi_2) + J_i(q_i\phi_2) < 0. \tag{A16b}$$

If $J_i \sim 0$, we get back from equation (A16a) the condition discussed above and equation (A16b) is satisfied identically since $j(\phi_2) < 0$ when the j_2 term is dominant. At zero potentials the ion fluxes are typically 2 orders of magnitude smaller than the electron fluxes, because of the smaller electron mass, and the approximation $J_i = 0$ is a good one. We are here assuming that we are below the asymptotic limit $\phi \to \infty$, where $j(\phi) \to 0$ and the flux is dominated by the positive ions. A net flux voltage curve, including the ions, is depicted in Figure 5. In Figure 5, point B is shown as the positive maximum at ϕ_1 and point C is the negative minimum at ϕ_2.

[57] The above analysis could be carried out with plasma densities n_N instead of fluxes, using the connecting relation

$$J_N = cn_N\sqrt{T_N}(\delta(T_N) + \eta(T_N) - 1), \tag{A17}$$

where c is a constant. In order to compute the secondary and backscatter coefficients, the material properties are needed.

[58] **Acknowledgments.** We would like to thank Michelle F. Thomsen for permission to use Figure 7. We are grateful to Frank Zimmermann for providing us with the *Cimino et al.* [2004] reference.

[59] Amitava Bhattacharjee thanks Spencer Kuo and another reviewer for their assistance in evaluating this paper.

References

Bransden, B. H., and C. J. Joachain (1989), *Introduction to Quantum Mechanics*, pp. 138–144, Longman, New York.

Cazaux, J. (2001), About the secondary electron yield and the sign of charging of electron irradiated insulators, *Euro. Phys. J. Appl. Phys.*, *15*, 167–172.

Cazaux, J. (2006), Electron-induced secondary electron emission yield of insulators and charged effects, *Nucl. Instrum. Methods Phys. Res. Sect. B*, *244*, 307–322.

Cimino, R., I. R. Collins, M. A. Furman, M. Pivi, F. Ruggerio, G. Rumulo, and F. Zimmermann (2004), Can low-energy electrons affect high-energy physics accelerators?, *Phys. Rev. Lett.*, *93*(1), 14,801–14,804, doi:10.1103/PhysRevLett.93.014801.

Darlington, E. H., and V. E. Coslett (1972), Backscattering of 0.5–10 keV electrons from solid targets, *J. Phys. D. Appl. Phys.*, *5*, 1969–1981.

Jablonski, A., and P. Jiricek (1996), Elastic electron backscattering from surfaces at low energies, *Surf. Interface Anal.*, *24*, 781–785,

doi:10.1002/(SICI)1096-9918(199610)24:11<781::AID-SIA187>3.0.CO;2-K.

Jablonski, A., J. Gryko, J. Kraser, and S. Tougaard (1989), Elastic electron backscattering from surfaces, *Phys. Rev. B*, *39*(1), 61–71.

Katz, I., M. Mandell, G. Jongeward, and M. S. Gussenhoven (1986), The importance of accurate secondary electron yields in modeling spacecraft charging, *J. Geophys. Res.*, *91*(A12), 13,739–13,744, doi:10.1029/JA091iA12p13739.

Laframboise, J. G., and M. Kamitsuma (1983), The Threshold temperature effect in high voltage spacecraft charging, *Rep. AFRL-TR-83-0046*, pp. 293–308, U.S. Air Force Res. Lab., Hanscom, Mass.

Laframboise, J. G., R. Godard, and M. Kamitsuma (1982), Multiple floating potentials, threshold temperature effects, and barrier effects in high voltage charging of exposed surfaces on spacecraft, in *Proceedings of International Symposium on Spacecraft Materials in Space Environment*, pp. 269–275, Eur. Space Agency, Paris.

Lai, S. T. (1991a), Spacecraft charging thresholds in single and double maxwellian space environments, *IEEE Trans. Nucl. Sci.*, *38*, 1629–1634, doi:10.1109/23.124155.

Lai, S. T. (1991b), Theory and observation of triple-root jump in spacecraft charging, *J. Geophys. Res.*, *96*(A11), 19,269–19,282, doi:10.1029/91JA01653.

Lai, S. T., and D. Della-Rose (2001), Spacecraft charging at geosynchronous altitudes: New evidence of the existence of critical temperature, *J. Spacecr. Rockets*, *38*(6), 922–928, doi:10.2514/2.3764.

Lai, S. T., and M. Tautz (2006), High-level spacecraft charging in eclipse at geosynchronous altitudes: A statistical study, *J. Geophys. Res.*, *111*, A09201, doi:10.1029/2004JA010733.

Lai, S. T., M. S. Gussenhoven, and H. A. Cohen (1982), Energy range of ambient electrons responsible for spacecraft charging, *Eos Trans. AGU*, *63*(18), 421.

Lai, S. T., M. S. Gussenhoven, and H. A. Cohen (1983), The concepts of critical temperature and energy cutoff of ambient electrons in high voltage charging of spacecraft, in *Proceedings of the 17th ESLAB Symposium*, edited by D. Guyenne and J. H. A. Pedersen, pp. 169–175, Eur. Space Agency, Noordwijk, Netherlands.

Lin, Y., and D. G. Joy (2005), A new examination of secondary electron yield data, *Surf. Interface Anal.*, *37*, 895–900, doi:10.1002/sia.2107.

Mayer, J. E., and M. G. Mayer (1963), *Statistical Mechanics*, John Wiley, New York.

Mott-Smith, H. M., and I. Langmuir (1926), The theory of collectors in gaseous discharge, *Phys. Rev.*, *28*, 727–763, doi:10.1103/PhysRev.28.727.

Prokopenko, S. M., and J. G. L. Laframboise (1980), High voltage differential charging of geostationary spacecraft, *J. Geophys. Res.*, *85*(A8), 4125–4131, doi:10.1029/JA085iA08p04125.

Reagan, J. B., R. E. Meyerott, R. W. Nightingale, P. C. Filbert, and W. L. Imhoff (1983), Spacecraft charging currents and their effects on space systems, *IEEE Trans. Electr. Insul.*, *EI-18*(2), 354–365, doi:10.1109/TEI.1983.298625.

Sanders, N. L., and G. T. Inouye (1978), Secondary emission effects on spacecraft charging: Energy distribution consideration, in *Spacecraft Charging Technology 1978*, edited by R. C. Finke and C. P. Pike, pp. 747–755, U.S. Air Force Geophys. Lab., Hanscom, Mass.

Sternglass, E. J. (1954a), Theory of secondary electron emission, *Sci. Pap. 1772*, Westinghouse Res. Lab., Pittsburgh, Pa.

Sternglass, E. J. (1954b), Backscattering of kilovolt electrons from solids, *Phys. Rev.*, *95*(2), 345–358, doi:10.1103/PhysRev.95.345.

Thomsen, M., E. Noveroske, J. Borovsky, and D. McComus (1999), Calculation of moments from measurements by the Los Alamos Magnetospheric Plasma Analyzer, *LANL Rep. LA-13566-MS*, Los Alamos Natl. Lab, Los Alamos, N.M.

S. T. Lai, Vehicles Directorate, Air Force Research Laboratory, Hanscom Air Force Base, 29 Randolph Road, Mail Stop VSBXT, Hanscom, MA 01731, USA. (afrl.rvb.pa@hanscom.af.mil)